The Canadian Mineralogist
Vol. 35, pp. 189-202 (1997)

PHASE TRANSITIONS IN THE SERIES BORACITE – TREMBATHITE – CONGOLITE: AN INFRARED SPECTROSCOPIC STUDY

PETER C. BURNS[1] AND MICHAEL A. CARPENTER

Department of Earth Sciences, University of Cambridge, Downing Street, Cambridge CB2 3EQ, U.K.

ABSTRACT

The marine-evaporite-hosted borate deposits at Sussex, New Brunswick, contain boracite-group minerals of the solid-solution series $Mg_3B_7O_{13}Cl$ – $Fe_3B_7O_{13}Cl$. At 25°C the orthorhombic structure (*Pca*2_1) is stable for compositions from $Mg_3B_7O_{13}Cl$ to $(Mg_{1.9}Fe_{1.1})B_7O_{13}Cl$, and the rhombohedral structure (*R*3*c*) occurs for compositions ranging from $(Mg_{1.9}Fe_{1.1})B_7O_{13}Cl$ to $Fe_3B_7O_{13}Cl$. At temperatures greater than 330°C, crystals of all compositions have the cubic boracite structure ($F\bar{4}3c$). Cooling results in a first-order phase transition to the orthorhombic structure, and specimens with more than 36 mol.% $Fe_3B_7O_{13}Cl$ undergo a further first-order phase transition to the rhombohedral structure. Samples of boracite, trembathite and congolite have been examined using both mid- and far-infrared absorption spectroscopy at 25°C and at high temperatures. This study suggests the existence of a previously unknown boracite-type phase in samples with Mg ≈ Fe over the temperature interval ~90 to 210°C. Phonons in the mid-infrared range are insensitive to composition, assuming that no phase transition has occurred, indicating that they are mainly due to vibrations in the borate framework. The far-infrared spectra vary considerably with composition, thus the modes are largely due to vibrations of the metal atoms. Phase transitions are readily discernible in either middle- or far-infrared spectra. The peak that occurs at ~1350 cm^{-1} is associated with an antisymmetric stretching mode of the BO_3 triangles; this peak is observed in all samples at all temperatures, demonstrating that the BO_3 triangles persist even in the cubic structure. As X-ray-diffraction studies indicate that the cubic structure contains BO_4 tetrahedra but not BO_3 triangles, the presence of the modes due to BO_3 triangles in the spectra corresponding to material with the cubic structure may be due to a dynamic disorder of boron and oxygen atoms, such that the average structure, as determined by X-ray diffraction, contains only BO_4 tetrahedra.

Keywords: boracite, trembathite, congolite, phase transition, infrared spectroscopy, solid solution, mineral physics.

SOMMAIRE

Les gisements de borate que contiennent les séquences évaporitiques marines à Sussex, au Nouveau-Brunswick, contiennent des minéraux du groupe de la boracite, membres de la solution solide $Mg_3B_7O_{13}Cl$ – $Fe_3B_7O_{13}Cl$. A 25°C, la structure orthorhombique (*Pca*2_1) est stable pour les compositions allant de $Mg_3B_7O_{13}Cl$ à $(Mg_{1.9}Fe_{1.1})B_7O_{13}Cl$, tandis que la structure rhomboédrique (*R*3*c*) est adoptée par les compositions allant de $(Mg_{1.9}Fe_{1.1})B_7O_{13}Cl$ à $Fe_3B_7O_{13}Cl$. A des températures supérieures à 330°C, les cristaux de n'importe quelle composition adoptent la structure de la boracite cubique ($F\bar{4}3c$). Un refroidissement mène à une inversion de premier ordre à la structure orthorhombique, et les échantillons contenant plus de 36% (base molaire) de $Fe_3B_7O_{13}Cl$ font preuve d'une inversion supplémentaire de premier ordre à une structure rhomboédrique. Nous avons examiné les échantillons de boracite, trembathite et congolite par spectroscopie d'absorption dans l'infra-rouge moyen et lointain à 25°C et à température élevée. Nous avons décelé l'existence d'une structure jusqu'ici méconnue dans le cas d'échantillons contenant des proportions à peu près équivalentes de Mg et de Fe sur un intervalle de température compris entre environ 90 et 210°C. Les phonons dans l'infra-rouge moyen semblent insensibles à la composition, si l'on suppose qu'aucune inversion n'a eu lieu, indication qu'ils sont surtout dus aux vibrations dans les groupes borate de la trame. Dans l'infra-rouge lointain, les spectres varient considérablement avec la composition, et les modes sont donc surtout attribuables aux vibrations des cations. Les inversions sont facilement repérables dans l'infra-rouge moyen ou lointain. Le pic que nous observons à environ 1350 cm^{-1} est associé à un mode d'étirement anti-symétrique des groupes triangulaires BO_3; ce pic est présent dans tous les échantillons et à toutes les températures, démontrant que ces groupes persistent même dans la structure cubique. Considérant que les études par diffraction X indiquent la présence de tétraèdres BO_4 dans la structure cubique, et non de triangles BO_3, la présence des modes attribués aux triangles BO_3 dans les spectres correspondant aux matériaux ayant la structure cubique pourrait bien témoigner d'un désordre dynamique du bore et des atomes d'oxygène, de sorte que la structure moyenne, telle que révélée par diffraction X, contient uniquement que des tétraèdres BO_4.

(Traduit par la Rédaction)

Mots-clés: boracite, trembathite, congolite, inversion, spectroscopie dans l'infra-rouge, solution solide, physique des minéraux.

[1] Current address: Department of Geology, University of Illinois at Urbana-Champaign, 245 Natural History Building, 1301 West Green Street, Urbana, Illinois 61801, U.S.A. *E-mail address*: pburns@hercules.geology.uiuc.edu

INTRODUCTION

Boracite-type phases, with the general formula $M_3B_7O_{13}X$ (M^{2+} = Mg, Cr, Mn, Fe, Co, Ni, Cu, Zn, Cd; X = Cl, Br, I), have been extensively studied, owing to the ferroelastic, ferroelectric and magnetic properties of the crystals (Nelmes 1974). These materials have structures with cubic symmetry at high temperatures, but upon cooling, most undergo phase transitions to ferroelastic and ferroelectric structures with lower symmetry. Most crystals of boracite-group minerals show complex twinning and anomalous optical properties that are due to the phase transitions. Five minerals belong to the boracite group (Table 1); all have Cl as the halogen, and four contain Mg and Fe as the divalent metal. However, Burns & Carpenter (1996) have demonstrated that, of these four, ericaite does not occur at room temperature.

The Penobsquis evaporite deposit, located at Sussex, New Brunswick, contains an extensive suite of borate minerals (Roulston & Waugh 1981, Rachlin *et al.* 1986, Mandarino *et al.* 1990, Burns *et al.* 1992, Roberts *et al.* 1993, Grice *et al.* 1994), which includes the boracite-group minerals boracite, trembathite and congolite in the series $Mg_3B_7O_{13}Cl$ – $Fe_3B_7O_{13}Cl$. The structure of boracite [$Mg_3B_7O_{13}Cl$] has orthorhombic symmetry ($Pca2_1$) at 25°C, whereas the structures of both trembathite [$(Mg,Fe)_3B_7O_{13}Cl$] and congolite [$(Fe,Mg)_3B_7O_{13}Cl$] have rhombohedral symmetry ($R3c$) at 25°C.

Burns & Carpenter (1996) have examined the phase relations in the solid solution $Mg_3B_7O_{13}Cl$ – $Fe_3B_7O_{13}Cl$ at 25°C and higher temperatures, using optical microscopy and X-ray powder-diffraction techniques; the results are summarized in Figure 1. At temperatures greater than 330°C, all specimens examined have the cubic boracite structure ($F\bar{4}3c$), and cooling results in a first-order phase transition to the orthorhombic structure. Specimens with more than 36 mol.% $Fe_3B_7O_{13}Cl$ undergo a further first-order phase transition to the rhombohedral structure. Burns & Carpenter (1996) found that the thermodynamic character of the phase transitions and the volume strain associated with it are dependent on a specimen's composition. Samples rich in Mg undergo a strongly first-order phase transition with the greatest volume strain, whereas increasing Fe results in a trend toward tricritical or second-order character, and coincides with a decrease in the absolute value of the volume strain due to the phase transition. In addition, the X-ray-diffraction data of Burns & Carpenter (1996) suggest that there may be an additional, unexpected phase transition to a previously unknown structure in material with roughly equivalent amounts of Mg and Fe.

Hard-mode spectroscopy has been shown to be a useful technique for the study of phase transitions (Bismayer 1988, Güttler 1990, Salje 1992). The vibrational spectra of numerous boracite-type phases have been reported, primarily from Raman spectroscopy (Lockwood 1974, 1976a, b, 1978, Lockwood & Murray 1978, Lockwood & Syme 1978, Arakelian & Hart 1987); Moopenn & Coleman (1990) reported an infrared spectroscopic study of the phase transitions in $Ni_3B_7O_{13}Br$ and $Cu_3B_7O_{13}Cl$ boracite. Both of these phases undergo first-order phase transitions from the $F\bar{4}3c$ structure to the $Pca2_1$ structure upon cooling. The cubic and orthorhombic boracite structures have 19 and 213 infrared-active vibrational modes, respectively (Moopenn & Coleman 1990). This huge increase in the number of modes at the phase transition makes the infrared spectra highly sensitive to the phase transitions in boracite-type phases. Here we present a reconnaissance infrared spectroscopic study of the $F\bar{4}3c \leftrightarrow Pca2_1$ and $Pca2_1 \leftrightarrow R3c$ phase transitions in the series $Mg_3B_7O_{13}Cl$ – $Fe_3B_7O_{13}Cl$.

TABLE 1. CELL DIMENSIONS OF BORACITE-GROUP MINERALS

		Space Group	a (Å)	b (Å)	c (Å)	Ref.
Boracite	$Mg_3B_7O_{13}Cl$	$Pca2_1$	8.577(6)	8.553(8)	12.09(1)	1
ericaite	$(Fe,Mg)_3B_7O_{13}Cl$	$Pca2_1$	8.58	8.65	12.17	2
trembathite	$(Mg,Fe)_3B_7O_{13}Cl$	$R3c$	8.574(2)		20.99(1)	3
congolite	$(Fe,Mg)_3B_7O_{13}Cl$	$R3c$	8.622(1)		21.054(5)	4
chambersite	$Mn_3B_7O_{13}Cl$	$Pca2_1$	8.68(1)	8.68(1)	12.26(1)	5

References: (1) Burns (1995); (2) Kühn & Schaacke (1955); (3) Burns *et al.* (1992); (4) Wendling *et al.* (1972); (5) Honea & Beck (1962).

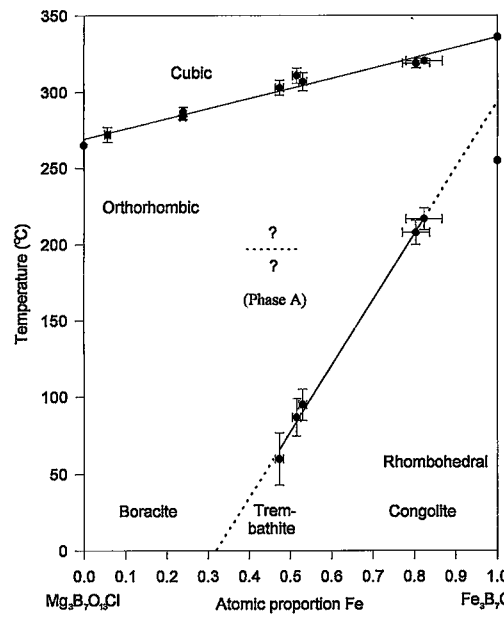

FIG. 1. Phase relations in the series boracite – trembathite – congolite, from Burns & Carpenter (1996). Data points with error bars are from the study by Burns & Carpenter (1996), data points without error bars are from Schmid & Tippmann (1978).

Crystal Structure

The cubic boracite structure (Ito *et al.* 1951, Sueno *et al.* 1973) consists of a framework of corner-sharing BO_4 tetrahedra, with metal and halogen atoms located in cavities in the borate framework. The structure is very unusual because it contains an oxygen atom [O(1) using the notation of Sueno *et al.* (1973)] that bonds to four boron atoms. This arrangement occurs only in the structure of cubic boracite-type phases. Presumably to prevent overbonding at the oxygen atom position, the four B(2)–O(1) bond-lengths are 1.69 Å (Sueno *et al.* 1973). Significant anisotropic thermal motion of the B(2) and O(1) atoms is observed. The structure reported by Sueno *et al.* (1973) pertains to the cubic form of $Mg_3B_7O_{13}Cl$. These authors argued that the refined atomic-displacement parameters are consistent with disorder of the Mg and Cl atoms in the cavities of the borate framework. However, Nelmes & Thornley (1973) provided a refinement of the cubic structure of $Cr_3B_7O_{13}Cl$, and argued that there is no evidence for any kind of disorder in *any* of the cubic phases of boracite for which structures have been reported. Instead, they concluded that significant thermal motion of the metal and halogen atoms occurs about a single potential minimum in each crystallographic site. Later structure refinements for cubic $Cu_3B_7O_{13}Cl$ (Thornley *et al.* 1976a), $Ni_3B_7O_{13}I$ (Thornley *et al.* 1976b, Nelmes & Thornley 1976), $Cu_3B_7O_{13}Br$ (Nelmes & Hay 1981), $Cu_3B_7O_{13}I$ (Nelmes & Hay 1981), $Cu_3B_7O_{13}Cl$ (Berset *et al.* 1985) and $Cr_3B_7O_{13}Cl$ (Monnier *et al.* 1987) support the conclusions of Nelmes & Thornley (1973).

In the low-temperature structures, the O(1) atom is bonded to only three boron atoms, and the borate framework contains *both* BO_3 triangles and BO_4 tetrahedra. At 25°C, the structure of boracite, $Mg_3B_7O_{13}Cl$, has orthorhombic symmetry, space group $Pca2_1$ (Dowty & Clark 1973), whereas the structures of congolite and trembathite have rhombohedral symmetry, space group $R3c$ (Schmid 1970, Mendoza-Alvarez *et al.* 1985, Burns *et al.* 1992). In each case, the coordination geometry of the metal atom is significantly distorted from the arrangement in the cubic structure, and the $Pca2_1$ and $R3c$ structures contain three and one symmetry-distinct metal sites, respectively. The structures also differ in the orientation of the BO_3 triangles. In the rhombohedral structure, the BO_3 triangles are coplanar and perpendicular to the three-fold axes, whereas in the orthorhombic structure, they are not coplanar, which explains why crystals with the rhombohedral structure have an optical birefringence that is large relative to that of crystals with the orthorhombic structure.

One important distinction between cubic and lower-symmetry boracite-type structures is that the high-symmetry structure contains only BO_4 tetrahedra, whereas the lower-symmetry structures contain both BO_3 triangles and BO_4 tetrahedra. Infrared and Raman spectroscopic measurements are sensitive to the presence of BO_3 groups. Where BO_3 triangles are present in a boracite-type structure, they give rise to an antisymmetric stretch mode at ~ 1350 cm^{-1}, and a weaker mode at ~1400 cm^{-1} that is due to the presence of ^{10}B, whose natural isotopic ratio to ^{11}B is 18:82 (Moopenn & Coleman 1990). Thus, it is possible to detect the persistence of BO_3 triangles in the cubic phase using spectroscopy. Moopenn & Coleman (1990) presented spectra for cubic $Ni_3B_7O_{13}Br$ and $Cu_3B_7O_{13}Cl$; the mode due to the antisymmetric stretching of the BO_3 triangle is not present in the spectrum of cubic $Ni_3B_7O_{13}Cl$, whereas it is a dominant feature in the lower-temperature spectra of the orthorhombic phase. In contrast, they found that the antisymmetric stretching mode of the BO_3 triangle is readily apparent in the spectrum of cubic $Cu_3B_7O_{13}Cl$, although the peaks are of much lower intensity than in the spectra for the orthorhombic phase. In addition, with heating of the orthorhombic structures of $Ni_3B_7O_{13}Br$ and $Cu_3B_7O_{13}Cl$, the full-width at half-maximum (FWHM) of the mode at ~1350 cm^{-1} is strongly temperature-dependent, suggesting a large anharmonic motion within the BO_3 group (Moopenn & Coleman 1990).

Experimental

Sample description

Four specimens were selected for study. Three of these are from sample suites from the Potash Company of Saskatchewan mine workings in the Penobsquis evaporite deposit at Sussex, New Brunswick. These sample suites are currently housed at the Canadian Museum of Nature (CMN) in Ottawa, Ontario. Each sample suite contains one or more sections of diamond-drill core from the Upper Halite Member (Roulston & Waugh 1983). Associated minerals are halite, hilgardite, hydroboracite, and the boracite-group minerals. Optical and X-ray-diffraction data collected at 25°C and at high temperatures, together with results of electron-microprobe analyses, are presented elsewhere (Burns & Carpenter 1996). The sample designated here as S4–IR is from CMN suite F93–20–4 and is a crystal selected from the same section of drill core as were samples S4A and S4B studied by Burns & Carpenter (1996). CMN suite F93–20–8 contains three sections of drill core; samples S8A–IR and S8E–IR were selected from two of these. Sample S8A–IR is from the same section of drill core as samples S8A and S8B studied by Burns & Carpenter (1996), whereas sample S8E–IR comes from the same section of drill core as samples S8D and S8E of Burns & Carpenter (1996). The fourth sample selected for study is near-end-member boracite from an unknown English locality. The sample, designated EB–IR, is from the same hand specimen as the sample EB studied by Burns & Carpenter (1996).

In each case, an inclusion-free crystal about 3 mm in diameter was selected for study. Each crystal was broken, and a portion was set aside for chemical analysis using an electron microprobe; the remainder was prepared for infrared absorption spectroscopy.

Infrared spectra

For infrared measurement, the crystals were ground by hand for approximately five minutes using an agate mortar and pestle. For mid-infrared absorption experiments, the standard pellet technique was used. Pellets were prepared by diluting the samples in KBr in ratios ~1:500. For far-infrared absorption experiments, the Si-wafer technique was used. The sample was prepared by gently pressing ~2.5 mg of sample onto a Si wafer using the back of a spatula, giving a sample area of ~1 cm^2.

The infrared absorption spectra were collected under vacuum using a Fourier transformation infrared spectrometer (Bruker IFS 113v). A liquid-nitrogen-cooled MCT detector was used for the mid-infrared range, and a room-temperature DTGS detector was used for the far-infrared range. A total of 350 scans were collected for each experiment. At the beginning of each day of experiments, reference spectra were collected for a blank KBr pellet or a Si wafer at all temperatures for which sample spectra were collected on that day. The sample was positioned in the middle of a cylindrical platinum-wound furnace in the sample compartment, and the temperature was permitted to stabilize for ten minutes before collecting each spectrum. The temperature was measured using a Pt–Rh thermocouple held in contact with the pellet. The temperature was controlled using a Eurotherm temperature-control system to a stability of ± 2°C. Under these experimental conditions, there is no possibility that a large thermal gradient exists across the pellet. On the basis of studies of the phase transitions in quartz and cristobalite, the temperature of the sample is accurate to within ±5°C. The spectral resolution was set to 2 cm^{-1} for mid-infrared and to 4 cm^{-1} for far-infrared ranges, respectively. The zero filling factor for the Fourier transform algorithm was 4 in order to enhance spectra features. It is possible that some Br ↔ Cl exchange between the KBr and the specimen occurred during the experiments. To minimize this possible effect, spectra were collected immediately after the pellets were prepared. Spectra collected at 25°C both before and after heating experiments were indistinguishable; thus, Br ↔ Cl exchange during the experiments was not detectable.

Electron-microprobe analysis

Crystal fragments were mounted in epoxy, polished, and coated with carbon for electron-microprobe analysis. Compositions were determined using a Cameca SX50 probe operated in wavelength-dispersion mode. The acceleration voltage was 20 kV, and the beam current was 15 nA; the samples were found to be stable under these conditions. The following standards were used: MgO (Mg), Fe metal (Fe), NaCl (Cl), Mn metal (Mn) and wollastonite (Ca). Multiple points were analyzed for each crystal; average values for each sample, along with the corresponding standard deviation, are reported in Table 2. The proportion of boron was calculated from stoichiometry.

RESULTS

Owing to the very large number of modes in the low-symmetry phases, no normal mode analysis has been attempted. However, considerable insight into the phase relations in the series $Mg_3B_7O_{13}Cl$ – $Fe_3B_7O_{13}Cl$ may be obtained by systematic comparisons of the spectra collected for each specimen. In general, the spectra are featureless at wave numbers above 1500 cm^{-1}. According to Moopenn & Coleman (1990), internal vibrational modes of the borate framework occur at wavenumbers above 200 cm^{-1}, whereas the modes below 200 cm^{-1} are mainly due to oscillations of the metal and halogen atoms.

Comparison of spectra collected for different specimens

As shown in Figure 1, all compositions should have a structure with cubic symmetry at temperatures above 330°C. The mid-infrared spectra collected at 400°C for each specimen are compared in Figure 2a. The spectra are very similar in appearance, and each contains about nine discernible peaks, with only minor variations in peak position and intensity apparent. This is entirely consistent with the conclusion of Burns & Carpenter

TABLE 2. CHEMICAL COMPOSITION OF BORACITE-GROUP MINERALS*

	EB-IR	S4-IR	S8A-IR	S8E-IR
# Points	36	30	40	39
FeO wt%	3.24(34)	12.40(29)	24.70(98)	34.85(1.74)
MnO	0.03(3)	0.90(5)	0.27(6)	0.75(10)
MgO	30.52(48)	22.16(46)	14.21(63)	6.49(1.26)
Cl	8.25(40)	8.47(6)	7.87(16)	7.65(8)
B_2O_3	65.21	59.71	56.86	53.33
Cl=O	-1.86	-1.91	-1.78	-1.73
Total	105.39	101.73	102.13	101.35
Fe^{2+}	0.17(2)	0.70(2)	1.47(6)	2.22(13)
Mn^{2+}	0.002(2)	0.052(3)	0.016(4)	0.048(7)
Mg	2.83(2)	2.24(2)	1.51(6)	0.73(13)
Cl	0.87(5)	0.97(1)	0.95(2)	0.99(1)

*B_2O_3 calculated from stoichiometry; formula calculations assume Mg + Fe + Mn = 3. Data obtained by electron-microprobe analysis.

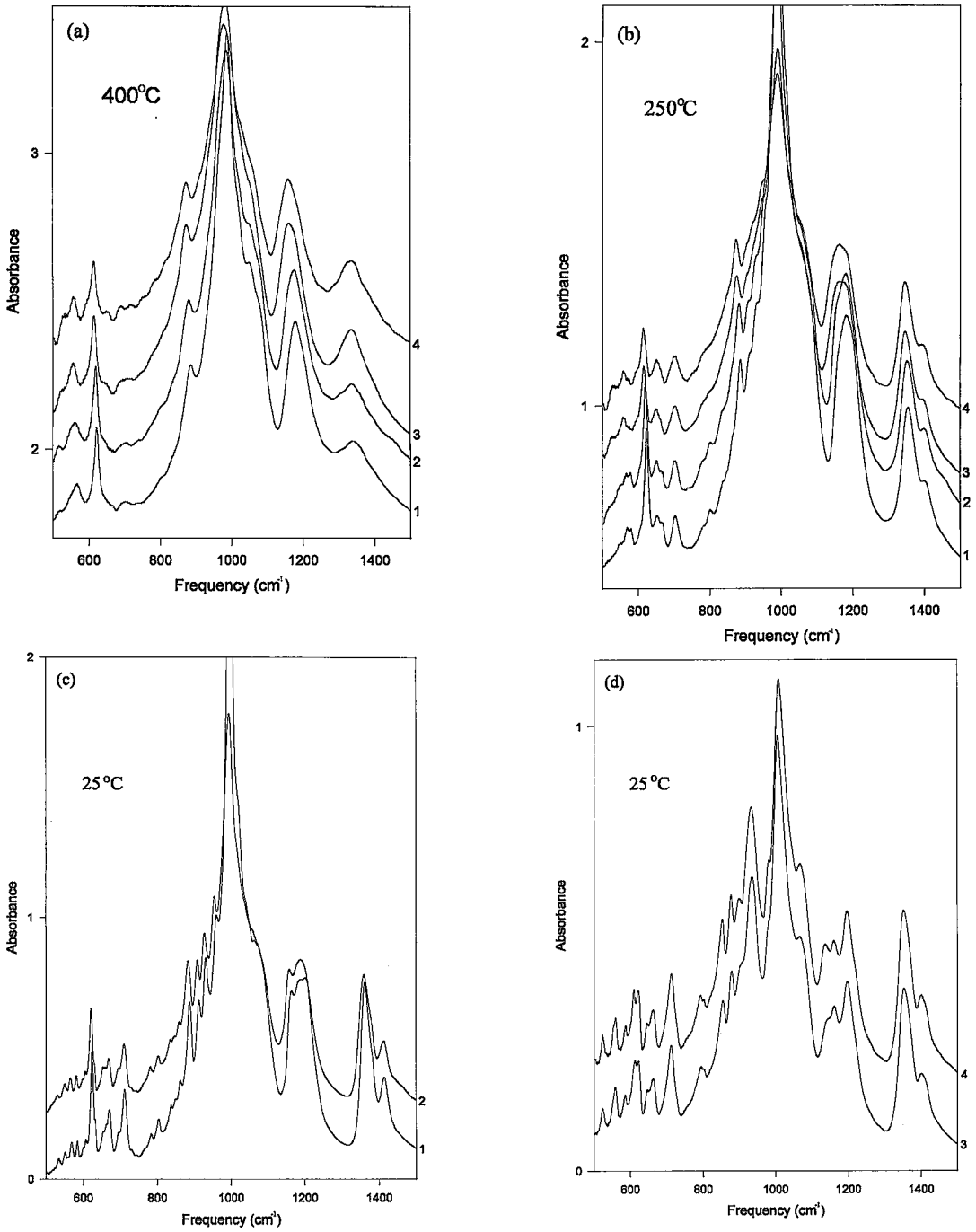

FIG. 2. Middle-infrared absorption spectra for samples: 1: EB–IR [M = $(Mg_{2.83}Fe_{0.17})$], 2: S4–IR [M = $(Mg_{2.24}Fe_{0.70}Mn_{0.05})$], 3: S8A–IR [$M$ = $(Mg_{1.51}Fe_{1.47}Mn_{0.02})$], 4: S8E–IR [$M$ = $(Fe_{2.22}Mg_{0.73}Mn_{0.05})$]. (a) Collected at 400°C, corresponding to the cubic structure. (b) Collected at 250°C (240°C in the case of sample EB–IR), corresponding to the orthorhombic structure. (c) Collected at 25°C, corresponding to the orthorhombic structure. (d) Collected at 25°C, corresponding to the rhombohedral structure. The absorbance is given in arbitrary units.

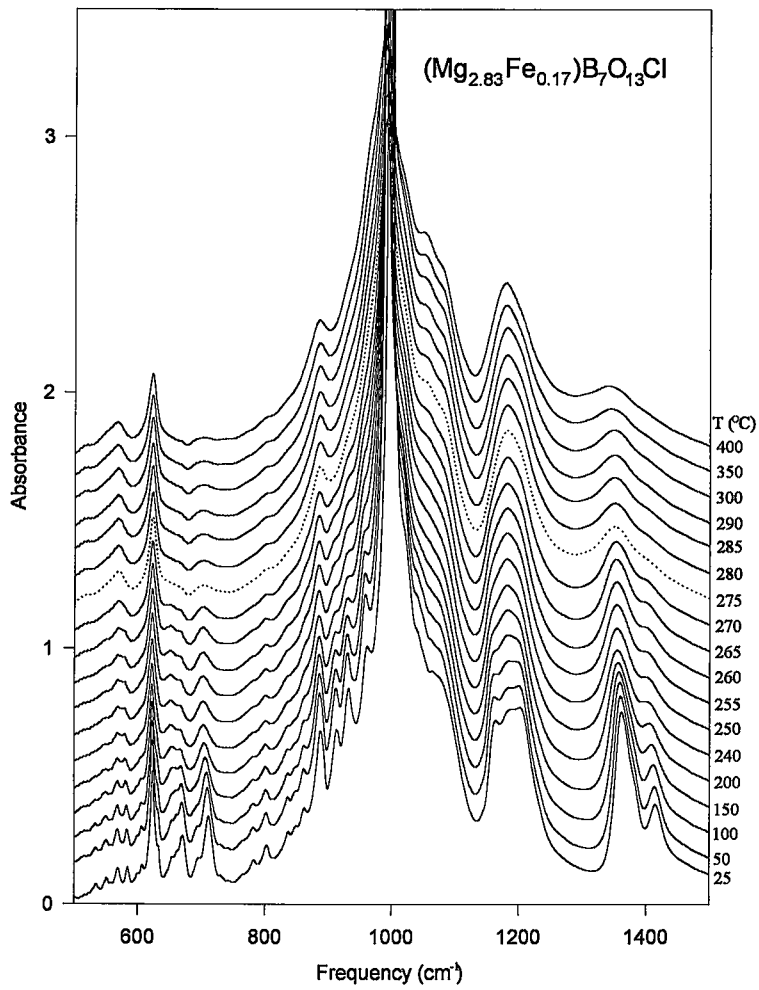

FIG. 3. Middle-infrared absorption spectra collected for sample EB–IR with M = $(Mg_{2.83}Fe_{0.17})$. The absorbance is given in arbitrary units.

(1996) that phases in the series $Mg_3B_7O_{13}Cl$ – $Fe_3B_7O_{13}Cl$ have a cubic structure at high temperatures. From Figure 1, it is also evident that each specimen should have orthorhombic symmetry at 250°C. Their middle-infrared spectra collected at this temperature (240°C in the case of sample EB–IR) are compared in Figure 2b. As expected, the spectra contain considerably more peaks than those for the cubic structure (Fig. 2a). The effect of composition appears only to be evident in details of peak position and intensity. On the basis of spectra shown in Figure 2b, it may be concluded that each sample has the same structure at 250°C.

At 25°C, samples with less than 36 mol.% $Fe_3B_7O_{13}Cl$ have the orthorhombic structure (EB–IR, S4–IR), whereas those with more than 36 mol.% $Fe_3B_7O_{13}Cl$ have the rhombohedral structure (S8A–IR, S8E–IR). The middle-infrared spectra collected at 25°C for samples EB–IR and S4–IR are compared in Figure 2c. They each contain about thirty-five distinguishable peaks, and the two spectra differ only in minor variations of the peak positions and intensities, confirming that the two samples have the same structure. They may be compared to the middle-infrared spectra of samples S8A–IR and S8E–IR, collected at 25°C and shown in Figure 2d. The spectra for the phases with rhombohedral symmetry (Fig. 2d) have about twenty-two discernable peaks, and the two spectra are very similar, except for minor variations in peak positions and intensities, which confirms that the samples are isostructural. At 25°C, the middle-infrared spectra of phases with orthorhombic (Fig. 2c) and rhombohedral (Fig. 2d) symmetry have the same general appearance, but close examination reveals that they differ significantly in terms of the number of peaks, their positions and relative intensities.

Comparison of spectra collected at different temperatures

Mid-infrared spectra were collected for each specimen over the temperature range 25°C to 400°C; in each figure, the spectra taken closest to the temperature of the phase transition (obtained using optical microscopy: Burns & Carpenter 1996) are indicated by dotted lines.

Consider first the spectra collected for samples EB–IR and S4–IR (Figs. 3, 4). Each of these specimens has an orthorhombic structure at 25°C, and upon heating, each undergoes a first-order transition to the cubic structure, with a reduction in the number of distinguishable peaks in the middle-infrared spectra (Figs. 3, 4). Many peaks are common to both structure types.

As noted above, the presence of BO_3 triangles gives rise to an antisymmetric stretch mode at ~1350 cm^{-1}, and a weaker mode at ~1400 cm^{-1}, due to the presence of ^{10}B. Both modes are clearly visible in the lower-temperature spectra for samples EB–IR and S4–IR (Figs. 3, 4), and it is also apparent that they persist into the cubic phase, even to 400°C. The variation of the position, FWHM and area of the peak at 1350 cm^{-1} in spectra taken for sample EB–IR is given in Figure 5. The frequency of the peak decreases continuously and linearly with increasing temperature in the orthorhombic phase, and there is an abrupt reduction of the frequency of the peak at the orthorhombic-to-cubic transition. The FWHM increases steadily as a function of temperature in the orthorhombic phase, and it abruptly increases at

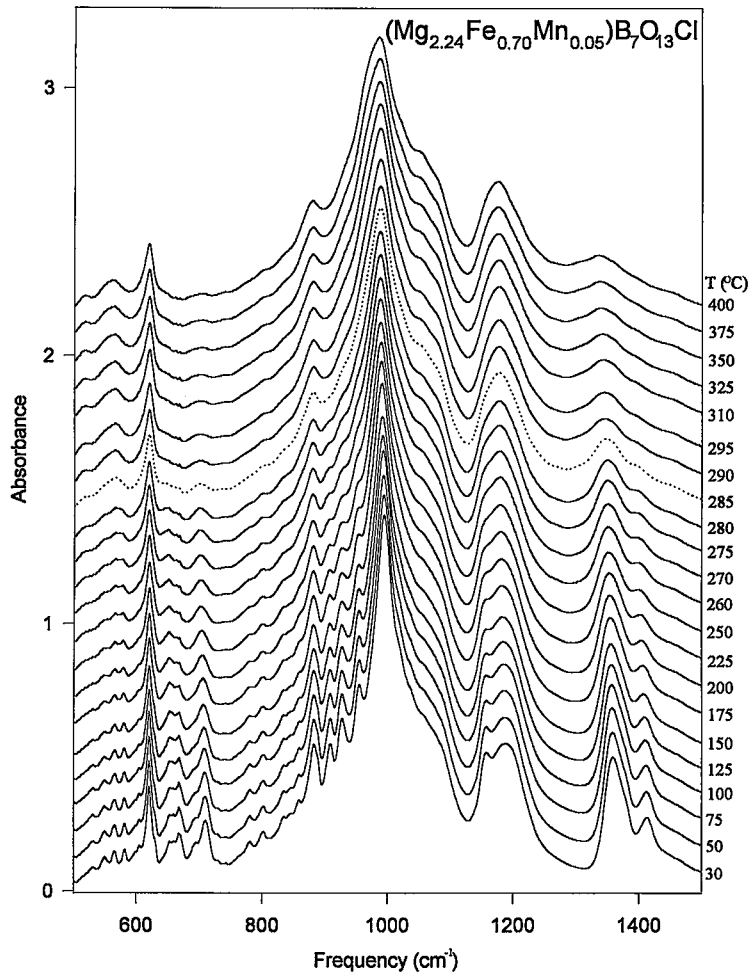

FIG. 4. Middle-infrared absorption spectra collected for sample S4–IR with M = $(Mg_{2.24}Fe_{0.70}Mn_{0.05})$. The absorbance is given in arbitrary units.

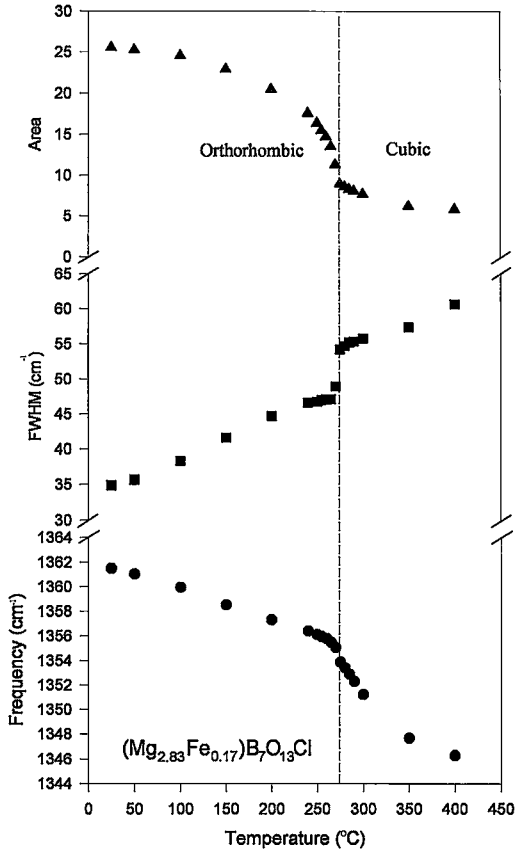

FIG. 5. The variation of the position, full-width at half-maximum (FWHM) and area of the peak at ~1350 cm^{-1} in spectra taken for sample EB–IR with $M = (Mg_{2.83}Fe_{0.17})$. This peak is due to an antisymmetric stretch mode of the BO_3 triangles. The units of area are arbitrary. The expected phase transition (from Fig. 1) is indicated by the broken line.

the onset of the cubic structure. The area of the peak decreases with increasing temperature, with an inflection point at the phase transition. All of these features are consistent with a first-order phase transition, as expected from previous work (Burns & Carptenter 1996, Schmid & Tippmann 1978, Dvořák & Petzelt 1971). The significant increase of the FWHM of the peak is indicative of strong anharmonic motion within the BO_3 triangle, which increases with increasing temperature. The very definite presence of this peak in the spectra corresponding to cubic structures indicates that BO_3 triangles do persist in the cubic phase of both of these specimens. This is inconsistent with the structural interpretations derived from X-ray-diffraction experiments.

Consider next the spectra collected for sample S8E–IR (Fig. 6). This specimen is rhombohedral at 25°C, and undergoes a first-order transition to the orthorhombic structure at ~205°C (from Fig. 1), and another first-order transition to the cubic structure at ~320°C. On cooling, the cubic-to-orthorhombic phase transition results in a significant increase in the number of peaks in the spectra (Fig. 6), whereas the phase transition from the orthorhombic to the rhombohedral structure is accompanied by a reduction of the number of peaks (Fig. 6). This is especially apparent in the region 900 cm^{-1} to 1000 cm^{-1}, which is shown enlarged in Figure 7.

The modes at ~1350 and ~1400 cm^{-1}, due to the antisymmetric stretch mode of the BO_3 triangle, are dominant features of spectra collected at all temperatures for sample S8E–IR. The dependence of the 1350 cm^{-1} peak position, FWHM and area upon temperature are given in Figure 8. The frequency of the peak gradually decreases with increasing temperature in both the rhombohedral and orthorhombic phases, with no significant discontinuity at the rhombohedral-to-orthorhombic transition. However, there is a significant decrease in the peak frequency at the onset of the cubic phase, and this first appears ~10°C below the phase transition (Fig. 8). The peak FWHM increases gradually from room temperature to ~300°C, and the trend shows an inflection point at the rhombohedral-to-orthorhombic transition. Above ~300°C, the FWHM begins to increase rapidly, and this continues once the structure has become cubic. The peak area decreases with increasing temperature, and shows a significant discontinuity at the rhombohedral-to-orthorhombic transition. The peak area decreases rapidly as the orthorhombic structure is heated, but becomes essentially constant with the onset of the cubic structure.

The spectra collected for sample S8A–IR are shown in Figure 9. This specimen is rhombohedral at 25°C, and a phase transition to a structure with a much lower optical birefringence occurs at ~90°C (Burns & Carpenter 1996). Although the phase stable above 90°C was designated orthorhombic by Burns & Carpenter (1996), they also noted, on the basis of a discontinuity in the unit-cell volume, that another phase transition may occur at ~200°C in specimens of this composition; thus there is uncertainty as to the symmetry of this phase. The structure becomes cubic at ~310°C. It was shown above (Fig. 2b) that all samples are isostructural at 250°C; on the basis of knowledge of the behavior of near-end-member boracite (EB–IR), we can unambiguously identify these spectra as corresponding to the orthorhombic structure. Examination of the spectra shown in Figure 9, and especially in the range 800 to 1100 cm^{-1} (Fig. 10), strongly supports the presence of a phase transition in this material at ~200°C. In particular, the single broad peak present in the spectra below 210°C at ~940 cm^{-1} collapses into several weaker modes at the transition. The presence of this transition is in accord with the discontinuity in unit-cell volume observed by Burns & Carpenter (1996), and requires the designation of a new phase in the temperature interval 90 to 210°C in samples with Mg ≈ Fe. This phase is provisionally designated phase *A*.

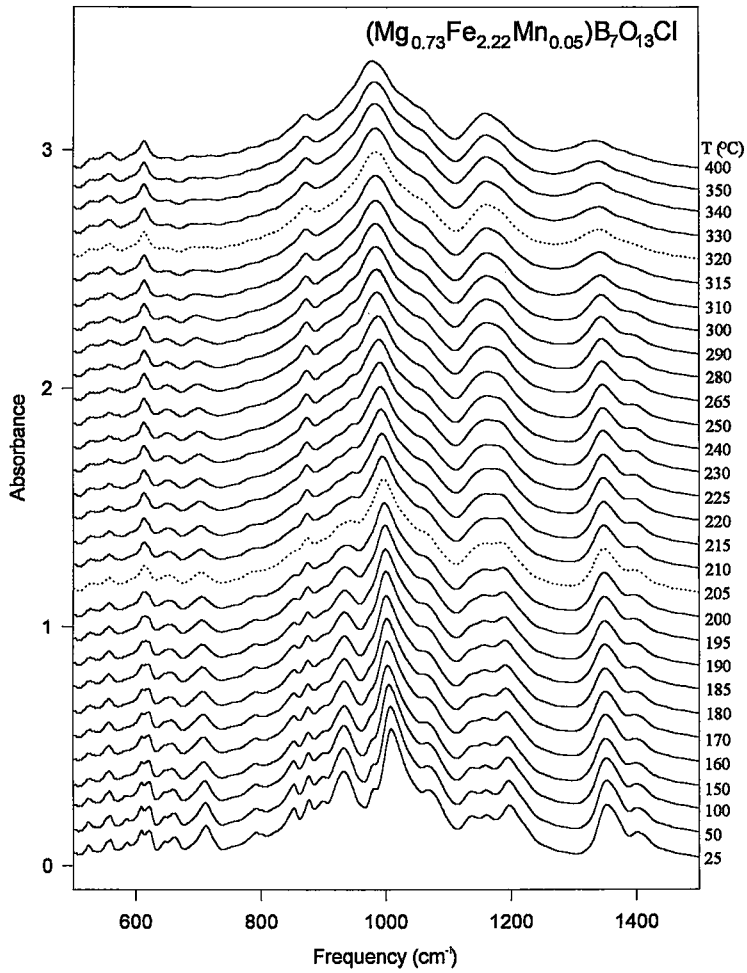

FIG. 6. Middle-infrared absorption spectra collected for sample S8E–IR with M = $(Mg_{0.73}Fe_{2.22}Mn_{0.05})$. The absorbance is given in arbitrary units.

Figure 11 shows the variation of the 1350 cm^{-1} peak position, FWHM, and area with temperature for sample S8A–IR. The peak frequency decreases continuously and smoothly with increasing temperature, with only a small discontinuity present at the transition from the orthorhombic to the cubic structure. The peak FWHM increases smoothly to ~300°C, with an increase in slope and a discontinuity at the onset of the cubic structure. The peak area decreases continuously, with an inflection point and change in slope at the orthorhombic-to-cubic transition. The rhombohedral - to - phase A and phase A - to - orthorhombic phase transitions are not evident in the trends for the peak at 1350 cm^{-1}.

The middle-infrared spectra for sample S8A–IR display only minor changes at the transition from the rhombohedral structure to phase A. There are slight variations in peak intensities and positions in general, and the peaks at 980 and 1140 cm^{-1} seem to be the most sensitive to this transition. However, it will not generally be possible to distinguish between the rhombohedral structure and phase A using mid-infrared spectra alone.

Far-infrared spectra

Spectra in the far-infrared region were collected for samples S8A–IR and S8E–IR over the temperature interval 25°C to 330°C. Consider first sample S8A–IR (Fig. 12). This sample has the rhombohedral structure from 25°C to the onset of phase A at ~90°C. The structure becomes orthorhombic at ~210°C, and cubic by ~310°C. The spectra are very complex, with at least fifteen different peaks. The phase transition from the rhombohedral structure to phase A is marked by several significant changes. A new peak appears at ~155 cm^{-1} and becomes more intense with increasing temperature. Also, peaks at ~355 and ~375 cm^{-1} vanish at the transition, whereas the frequency of the peak at ~398 cm^{-1},

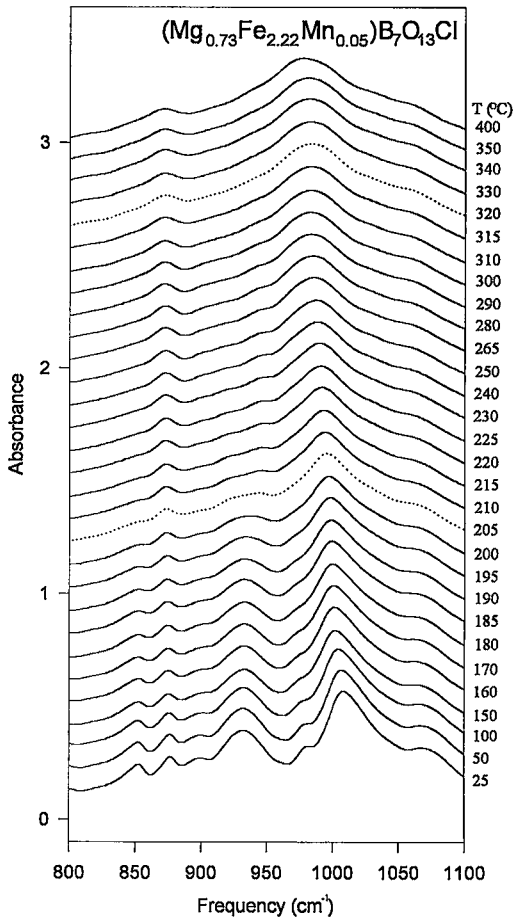

FIG. 7. An expanded portion of the middle-infrared absorption spectra collected for sample S8E–IR with M = ($Mg_{0.73}Fe_{2.22}Mn_{0.05}$). The absorbance is given in arbitrary units.

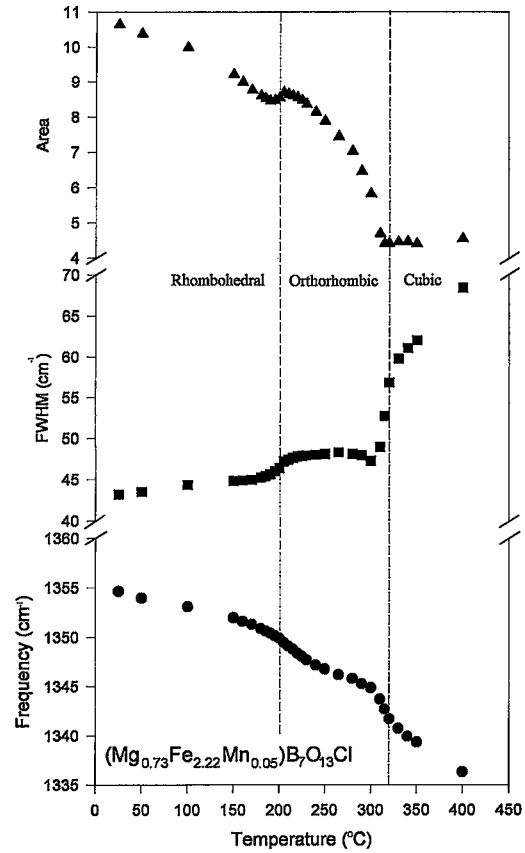

FIG. 8. The variation of the position, full-width at half-maximum (FWHM) and area of the peak at ~1350 cm^{-1} in spectra taken for sample S8E–IR with M = ($Mg_{0.73}Fe_{2.22}Mn_{0.05}$). This peak is due to an antisymmetric stretch mode of the BO_3 triangles. The units of area are arbitrary. Expected phase transitions (from Fig. 1) are indicated by broken lines.

which was essentially invariant in spectra for the rhombohedral structure, begins to decrease significantly at the transition to phase *A* (Fig. 13).

The phase transition from phase *A* to the orthorhombic structure in sample S8A–IR is also readily detected using far-infrared spectroscopy. As can be seen in Figure 12, several abrupt changes occur in the spectra at ~210°C. The peak at ~165 cm^{-1}, which had been a dominant feature in the lower-temperature spectra, is greatly reduced in intensity by 210°C, and is no longer present in spectra collected for temperatures above 210°C. The two peaks present at ~220 and ~250 cm^{-1} merge into one broad peak, and new peaks appear at ~355 and ~465 cm^{-1}; the peak at ~398 cm^{-1} becomes very broad, and vanishes by 290°C.

The far-infrared spectra collected for sample S8E–IR also contain about fifteen distinguishable peaks (Fig. 14). This sample has a rhombohedral structure from 25°C to ~210°C, which is the onset of the orthorhombic structure. The phase transition is readily detected in the spectra. At the onset of the orthorhombic structure, peaks at ~165 and 375 cm^{-1} vanish, peaks at ~230 and ~250 cm^{-1} merge into a single broad peak, as do the peaks at ~430 and ~450 cm^{-1}, the peak at ~355 cm^{-1} vanishes, a new peak appears at ~365 cm^{-1}, the peak at ~400 cm^{-1} becomes very broad and rapidly decreases in frequency, and a new peak appears at ~475 cm^{-1}.

DISCUSSION

The infrared spectra, especially in the far-infrared region, are quite sensitive to the phase transitions in the series $Mg_3B_7O_{13}Cl$ – $Fe_3B_7O_{13}Cl$. At 25°C, samples of the series $Mg_3B_7O_{13}Cl$ – $Fe_3B_7O_{13}Cl$ have either an orthorhombic or rhombohedral structure, and these polymorphs may be readily distinguished on the basis of spectra in either the mid- or far-infrared region. Comparison of spectra collected for samples with different

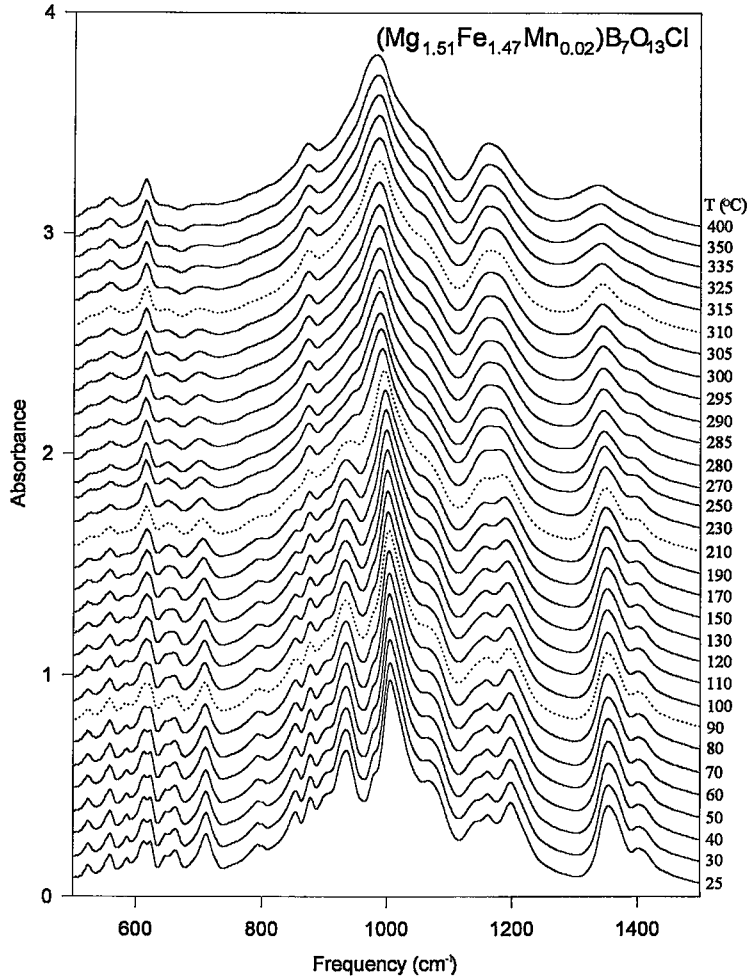

FIG. 9. Middle-infrared absorption spectra collected for sample S8A–IR with M = $(Mg_{1.51}Fe_{1.47}Mn_{0.02})$. The absorbance is given in arbitrary units.

compositions, but at the same temperature, shows that the mid-infrared region is not significantly affected by Mg ↔ Fe substitution, in the absence of a phase transition. This is consistent with the fact that the modes in this region are due mainly to vibrations within the borate framework. The spectra in the far-infrared region do vary significantly with composition, as the modes associated with the metal and halogen atoms are found in this region.

The persistence of BO_3 triangles at temperatures well above the cubic-to-orthorhombic phase transition has been indicated by the presence of peaks at ~1350 and ~1400 cm^{-1} in the infrared spectra. This result is at odds with X-ray-diffraction studies, which give a cubic structure containing BO_4 tetrahedra but not BO_3 triangles. Note, however, that a structure refinement has not been reported for a cubic phase of intermediate composition in the series $Mg_3B_7O_{13}Cl$ – $Fe_3B_7O_{13}Cl$. Also, it is common for boracite-type crystals to remain weakly anisotropic, even in the cubic phase (Nelmes 1974). Optical examination of the crystals studied here has shown them to be weakly anisotropic to temperatures exceeding 500°C.

The presence of the antisymmetric stretch mode of the BO_3 triangle at ~1350 and ~1400 cm^{-1} in spectra collected for phases with the cubic structure supports a model that involves a dynamic disorder of the B(2) and O(1) atoms. Such disorder is reflected by the very substantial broadening of these peaks with increasing temperature. The peaks begin to broaden well below the onset of the cubic phase, indicating that the dynamic motion of these atoms becomes significant in the stability field of the orthorhombic structure. X-ray-diffraction studies of the cubic structure of $Mg_3B_7O_{13}Cl$ (Sueno *et al.* 1973) give large anisotropic displacement parameters for both the B(2) and O(1) atoms, and this

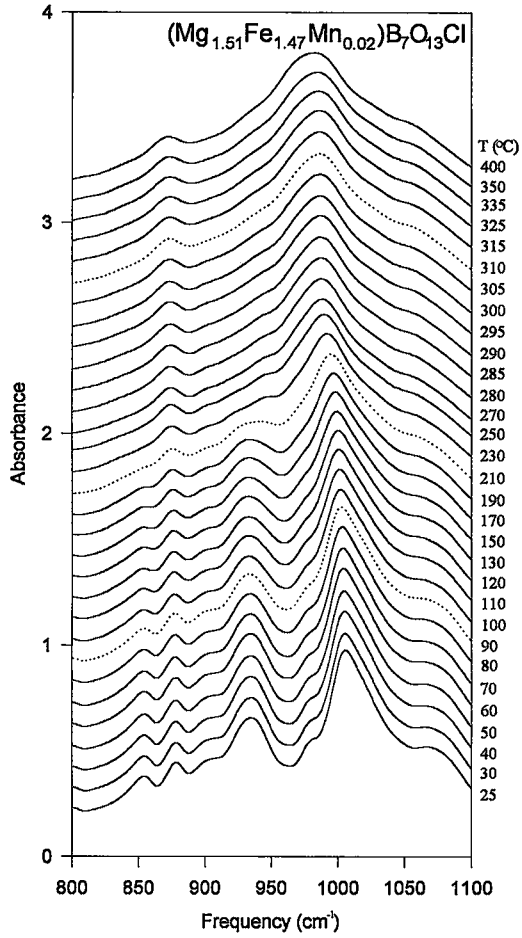

FIG. 10. An expanded portion of the middle-infrared absorption spectra collected for sample S8A–IR with M = $(Mg_{1.51}Fe_{1.47}Mn_{0.02})$. The absorbance is given in arbitrary units.

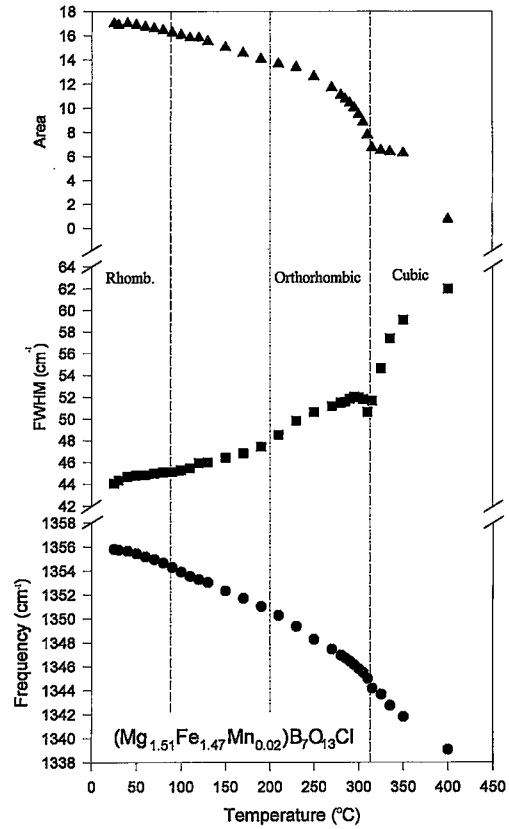

FIG. 11. The variation of the position, full-width at half-maximum (FWHM) and area of the peak at ~1350 cm^{-1} in spectra taken for sample S8A–IR with M = $(Mg_{1.51}Fe_{1.47}Mn_{0.02})$. This peak is due to an antisymmetric stretch mode of the BO_3 triangles. The units of area are arbitrary. Expected phase transitions (from Fig. 1) are indicated by broken lines.

is also the case for other cubic boracite-type structures. This disorder must occur in such a way that BO_3 triangles occur locally in the structure.

The existence of a new structure, phase *A*, in samples with Mg ≈ Fe over the temperature interval ~90 to ~210°C, is consistent with the systematic variations shown by the spectra. In the mid-infrared range, the spectra of the new phase are very similar to those of specimens with the rhombohedral structure, indicating that the borate framework of the structure of phase *A* must be quite similar to that of the rhombohedral structure. However, the lower optical birefringence of phase *A* relative to crystals with the rhombohedral structure suggests that the BO_3 triangles are not all coplanar in the structure of phase *A*, whereas they are so in the rhombohedral structure. Most differences between the spectra of phase *A* and the spectra for the rhombohedral material are in the far-infrared region, which is largely due to vibrations of the metal and halogen atoms (Moopenn & Coleman 1990). Phase *A* is presumably distinct because of a new arrangement of metal atoms in the structure, therefore, and this is in some way related to the apparent requirement of Mg ≈ Fe. Samples with different intermediate compositions are needed to define the stability field of this structural variant. It does not extend as far as $(Mg_{2.24}Fe_{0.70}Mn_{0.05})B_7O_{13}Cl$ (the composition of S4–IR), however.

ACKNOWLEDGEMENTS

The Natural Sciences and Engineering Research Council of Canada supported this work with a Post-Doctoral Fellowship to PCB. Clare Hall, Cambridge, supported PCB with a Research Fellowship. This manuscript was significantly improved following re-

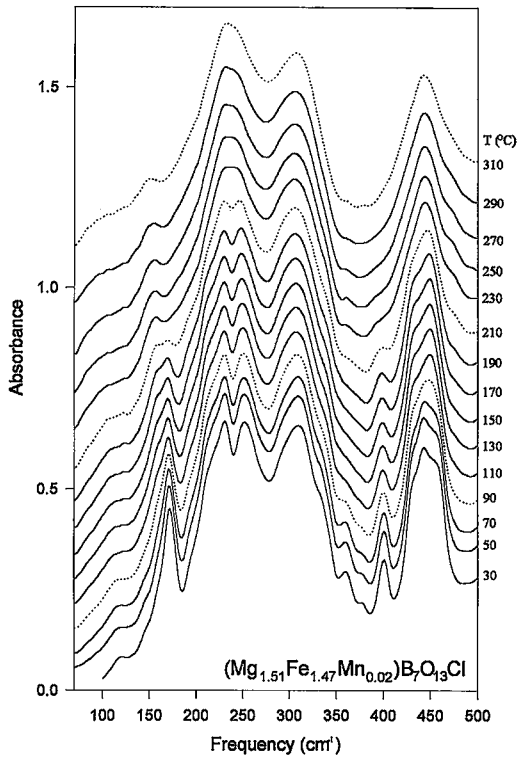

FIG. 12. Far-infrared absorption spectra collected for sample S8A–IR with M = ($Mg_{1.51}Fe_{1.47}Mn_{0.02}$). The absorbance is given in arbitrary units.

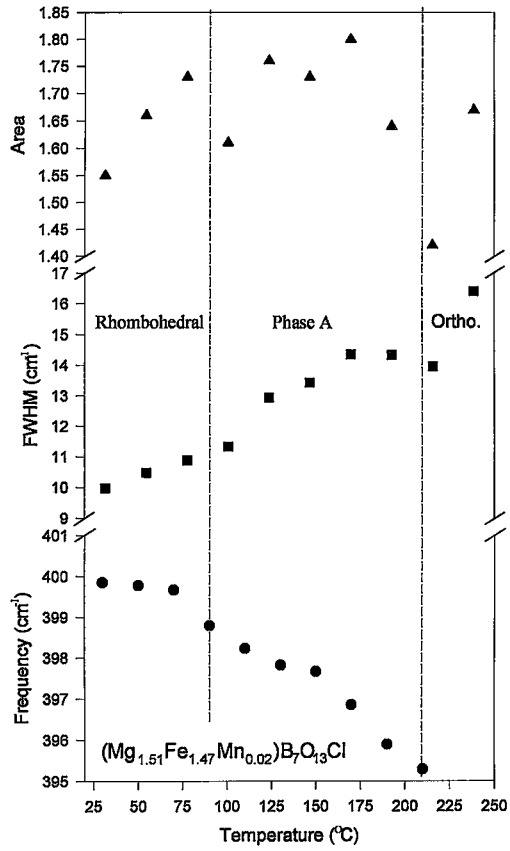

FIG. 13. The variation of the position, full-width at half-maximum (FWHM) and area of the peak at ~398 cm^{-1} in spectra taken for sample S8A–IR with M = ($Mg_{1.51}Fe_{1.47}Mn_{0.02}$). The units of area are arbitrary. Expected phase transitions (from Fig. 1) are indicated by broken lines.

views by Dr. A.M. Hofmeister and an anonymous referee, and editorial work by Dr. R.F. Martin.

REFERENCES

ARAKELIAN, H.E. & HART, T.R. (1987): Improper ferroelectric phase transition in magnesium chloride boracite. *Ferroelectrics* **74**, 13-21.

BERSET, G., DEPMEIER, W., BOUTELLIER, R. & SCHMID, H. (1985): Structure of boracite $Cu_3B_7O_{13}I$. *Acta Crystallogr.* **C41**, 1694-1696.

BISMAYER, U. (1988): New developments in Raman spectroscopy on structural phase transitions. *In* Physical Properties and Thermodynamic Behaviour of Minerals (E.K.H. Salje, ed.). *NATO Advanced Study Inst.* **C 225**, 143-183. Reidel, Dordrecht, The Netherlands.

BURNS, P.C. (1995): X-ray powder diffraction data for the identification of boracite-group minerals. *Powd. Diff.* **10**, 250-260.

_____ & CARPENTER, M.A. (1996): Phase transitions in the series boracite – trembathite – congolite: phase relations. *Can. Mineral.* **34**, 881-892.

_____, HAWTHORNE, F.C. & STIRLING, J.A.R. (1992): Trembathite, $(Mg,Fe)_3B_7O_{13}Cl$, a new borate mineral from the Salt Springs potash deposit, Sussex, New Brunswick. *Can. Mineral.* **30**, 445-448.

DOWTY, E. & CLARK, J.R. (1973): Crystal-structure refinements for orthorhombic boracite, $Mg_3ClB_7O_{13}$, and a trigonal, iron-rich analogue. *Z. Kristallogr.* **138**, 64-99.

DVOŘÁK, V. & PETZELT, J. (1971): Symmetry aspects of the phase transitions in boracites. *Czech. J. Phys.* **B21**, 1141-1152.

GRICE, J.D., BURNS, P.C. & HAWTHORNE, F.C. (1994): Determination of the megastructures of the borate polymorphs pringleite and ruitenbergite. *Can. Mineral.* **32**, 1-14.

GÜTTLER, B. (1990): Elastic phase transitions in minerals and hard mode infared spectroscopy – some examples. *In* Phase Transitions in Ferroelastic and Co-elastic Crystals (E.K.H. Salje, ed.). Cambridge University Press, Cambridge, U.K. (230-252).

HONEA, R.M. & BECK, F.R. (1962): Chambersite, a new mineral. *Am. Mineral.* **47**, 665-671.

ITO, T., MORIMOTO, N. & SADANAGA, R. (1951): The crystal structure of boracite. *Acta Crystallogr.* **4**, 310-316.

KÜHN, R. & SCHAACKE, I. (1955): Vorkommen und Analyse der Boracit- und Ericaitkristalle aus dem Salzhorst von Wathlingen-Hänigsen. *Kali und Steinsalz* **11**, 33-42.

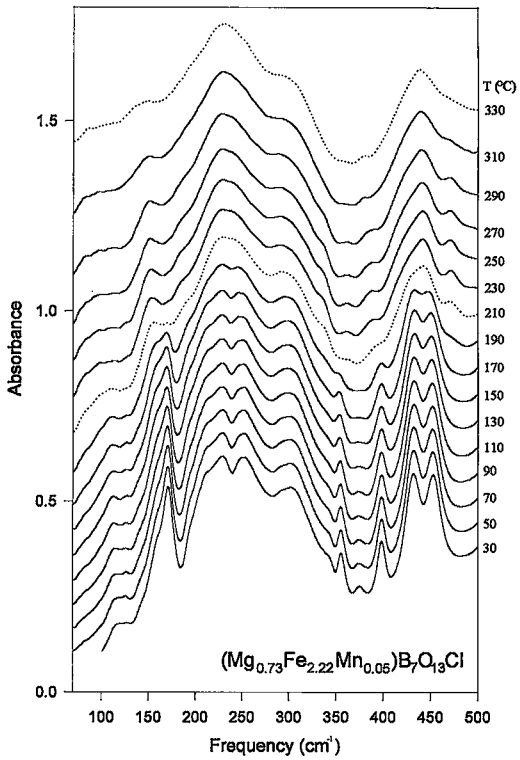

FIG. 14. Far-infrared absorption spectra collected for sample S8E–IR with M = ($Mg_{0.73}Fe_{2.22}Mn_{0.05}$). The absorbance is given in arbitrary units.

LOCKWOOD, D.J. (1974): Isolating the totally symmetric Raman spectrum of cubic crystals: the A_1 spectrum of $Cr_3B_7O_{13}Cl$. *J. Raman Spectros.* **2**, 555-562.

_____ (1976a): Raman spectral study of the ferroelectric phase transition in boracites. *Ferroelectrics* **13**, 353-354.

_____ (1976b): Observation of soft modes in the Raman spectrum of ferroelectric $Cr_3B_7O_{13}Cl$. *Solid State Comm.* **18**, 115-117.

_____ (1978): Raman spectrum of the orthorhombic phase of the improper ferroelectric manganese-chlorine boracite. *Indian J. Pure Appl. Phys.* **16**, 268-276.

_____ & MURRAY, A.F. (1978): Lattice dynamics of nickel-iodine boracite. *Ferroelectrics* **21**, 319-320.

_____ & SYME, R.W.G. (1978): Raman study of the ferroelectric phase transition in copper-chlorine boracite. *Ferroelectrics* **21**, 557-558.

MANDARINO, J.A., RACHLIN, A.L., DUNN, P.J., LE PAGE, Y., BACK, M.E., MUROWCHICK, B.L., RAMIK, R.A. & FALLS, R.B. (1990): Redefinition of volkovskite and its description from Sussex, New Brunswick. *Can. Mineral.* **28**, 351-356.

MENDOZA-ALVAREZ, M.-E., YVON, K., DEPMEIER, W. & SCHMID, H. (1985): Structure refinement of trigonal iron-chlorine boracite. *Acta Crystallogr.* **C41**, 1551-1552.

MONNIER, A., BERSET, G. & SCHMID, H. (1987): Cubic structure of chromium iodine boracite. *Acta Crystallogr.* **C43**, 1243-1245.

MOOPENN, A. & COLEMAN, L.B. (1990): Vibrational spectroscopy and the improper phase transition in nickel bromide and copper chloride boracite. *J. Phys. Chem. Solids* **51**, 1099-1110.

NELMES, R.J. (1974): Structural studies of boracites. A review of the properties of boracites. *J. Phys. C: Solid State Phys.* **7**, 3840-3854.

_____ & HAY, W.J. (1981): Structural studies of boracites. VI. The cubic phase of cobalt iodine boracite, $Co_3B_7O_{13}I$, and of copper bromine boracite, $Cu_3B_7O_{13}Br$. *J. Phys. C: Solid State Phys.* **14**, 5247-5257.

_____ & THORNLEY, F.R. (1973): Structural studies of boracites. The cubic phase of chromium chlorine boracite, $Cr_3B_7O_{13}Cl$. *J. Phys. C: Solid State Phys.* **7**, 3855-3874.

_____ & _____ (1976): Structural studies of boracites. III. The cubic phase of nickel iodine boracite, $Ni_3B_7O_{13}I$, at room temperature. *J. Phys. C: Solid State Phys.* **9**, 665-680.

RACHLIN, A.L., MANDARINO, J.A., MUROWCHICK, B.L., RAMIK, R.A., DUNN, P.J. & BACK, M.E. (1986): Mineralogy of hilgardite-4*M* from evaporites in New Brunswick. *Can. Mineral.* **24**, 689-693.

ROBERTS, A.C., STIRLING, J.A.R., GRICE, J.D., BURNS, P.C., ROULSTON, B.V., CURTIS, J.D. & JAMBOR, J.L. (1993): Pringleite and ruitenbergite, polymorphs of $Ca_9B_{26}O_{34}(OH)_{24}Cl_4{\cdot}13H_2O$, two new mineral species from Sussex, New Brunswick. *Can. Mineral.* **31**, 795-800.

ROULSTON, B.V. & WAUGH, D.C.E. (1981): A borate mineral assemblage from the Penobsquis and Salt Springs evaporite deposits of southern New Brunswick. *Can. Mineral.* **19**, 291-301.

_____ & _____ (1983): Stratigraphic comparison of the Mississippian potash deposits in New Brunswick, Canada. *Sixth International Symposium on Salt* **1**, 115-127.

SALJE, E.K.H. (1992): Hard mode spectroscopy: experimental studies of structural phase transitions. *Phase Transitions* **37**, 83-110.

SCHMID, H. (1970): Trigonal boracites – a new type of ferroelectric and ferromagnetoelectric that allows no 180° electric polarization reversal. *Phys. Stat. Sol.* **37**, 209-223.

_____ & TIPPMANN, H. (1978): Spontaneous birefringence in boracites – measurements and applications. *Ferroelectrics* **20**, 21-36.

SUENO, S., CLARK, J.R., PAPIKE, J.J. & KONNERT, J.A. (1973): Crystal-structure refinement of cubic boracite. *Am. Mineral.* **58**, 691-697.

THORNLEY, F.R., KENNEDY, N.S.J. & NELMES, R.J. (1976b): Structural studies of boracites. IV. Thermal motion in cubic $Ni_3B_7O_{13}I$ at 77K. *J. Phys. C: Solid State Phys.* **9**, 681-692.

_____, NELMES, R.J. & KENNEDY, N.S.J. (1976a): Structural studies of Cu–Cl-boracite. *Ferroelectrics* 13, 357-359.

WENDLING, E., HODENBERG, R.V. & KÜHN, R. (1972): Congolit, der trigonale Eisenboracit. *Kali und Steinsalz* **6**, 1-3.

Received March 14, 1996, revised manuscript accepted October 7, 1996.